

# A COLLIMATION EXPERIMENT WITH PROTONS AT 120GeV

N. Catalan Lasheras, G. Ferioli, J.B. Jeanneret, CERN, Geneva, Switzerland

## Abstract

We present the preliminary results of a two-stage collimation experiment made with a 120 GeV/c coasting proton beam in the SPS at CERN.

## 1 INTRODUCTION

In high intensity proton colliders with superconducting magnets, quenches induced by beam losses are unavoidable in the absence of a collimation system. It was shown that a single stage collimator system cannot suffice at TeV energies [1][2]. While the principles of a two-stage collimation system treated as an optical system are now well understood [3][4][5], a quantitative approach of its efficiency considering true scattering in collimator jaws has not yet been demonstrated. In this paper, we present the preliminary results of a two-stage collimation experiment done with a 120 GeV/c coasting beam in the SPS ring. The results are compared to a simulation code, which is used to evaluate the efficiency of the collimation system of LHC.

## 2 AIM OF THE EXPERIMENT

If a proton impacts the jaw of a collimator at a distance  $b$  from its inner edge which is smaller than a critical value  $b_c$  it has a good probability to be scattered back into the aperture of the ring before being absorbed. Neglecting nuclear elastic scattering, the critical impact parameter  $b_c$  is the r.m.s transverse deviation of a proton by multiple coulomb scattering (see Section 4.1) after one nuclear absorption length  $\lambda_{abs}$ . The result,

$$b_c = 5.2/p \text{ } [\mu\text{m, TeV}] \quad (1)$$

is Z-independent for metals to a good precision [2] while in a TeV proton collider with good operational conditions the impact parameter of the halo is expected to be in the  $\mu\text{m}$  range [2] justifying the use of secondary collimators. Then, whenever a reduction of the halo by several orders of magnitude is needed, the outscattering rate at secondary collimators becomes important too.

A measurement of the density of protons in phase-space after scattering requires the use of high precision telescopes inside the vacuum chamber while numerous inelastic particles produced in the thick jaws would hide the elastic signal. We therefore chose to measure the rate of inelastic collisions in all the jaws, while varying their relative transverse positions to give a wide basis for comparing simulations and measurements. We use basically two-jaws primary and secondary collimators, while a tertiary one is used as an analyser and plays the role of a variable ring aperture limitation.

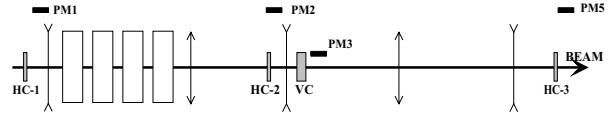


Figure 1: The layout of the SPS collimation experiment.

## 3 THE EXPERIMENT

The experiment was made in the SPS accelerator. We used the well understood mode of operation of a coasting proton beam at 120 GeV/c. Its intensity corresponded to  $N_p \approx 10^{12}$ p. The beam was debunched and made to slowly diffuse transversely by injecting some wideband noise in the kHz range with a horizontal kicker. The noise level was adjusted to set the loss rate to  $\dot{n}_{loss} \approx 5 \cdot 10^8 \text{ps}^{-1}$  and the impact parameter of the diffusing protons into the range  $b \leq 0.5 \mu\text{m}$  [6]. Three horizontal collimators ( $HC1,2,3$  in Figure 1) were installed in a weakly radioactive straight section. They are made of two opposite 250 mm long Aluminum jaws. The phase advance between collimators was  $\mu_{1-2} = 90^\circ$  and  $\mu_{1-3} = 200^\circ$ . The choice of Aluminum is discussed in Section 3.1. The length of the jaws corresponds to  $\sim 2/3$  of a nuclear absorption length, to allow for a large enough residual rate of inelastic interactions in the tertiary collimator. For hardware reasons, the tanks had to be installed near quadrupoles, fixing their relative phases advances near  $90^\circ$ . The phase advance  $\mu_{1-3}$  was chosen to avoid a point to point configuration between  $HC1$  and  $HC3$ , allowing the tertiary collimator to catch protons emitted at both  $HC1$  and  $HC2$ . A vertical collimator, made of two  $4 \lambda_{abs}$  jaws (stainless steel), was installed at  $\mu_{1-v} = 90^\circ$  to catch vertically scattered protons.

### 3.1 Detection of inelastic interactions

Secondary particles produced by inelastic interactions develop a shower in thick targets. A detailed simulation with the code GEANT [8] allowed to compute the energy deposition per inelastic interaction in scintillation counters ( $35 \times 1 \text{ cm}^3$ ) placed near the collimators. Most particles are emitted at small angles but a few low energy ones escape at large angle. Simulated analog spectra of energy deposition in the counters are shown in Figure 2. With Aluminum jaws, minimum ionising electrons traverse the full thickness of the scintillator and populate the second peak. Low energy atomic electrons and photoelectrons populate the first peak. With higher  $Z$  material to which correspond higher bremsstrahlung and photoelectric cross-sections, low energy particles dominate, hiding the minimum ionising peak. To best control the calibration of the counters, Aluminum was chosen and a threshold for counting was fixed

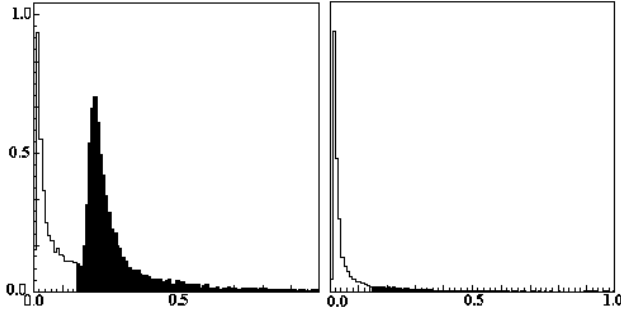


Figure 2: The analog spectrum of the scintillators as simulated with GEANT with a jaw made of aluminum (left) and of stainless steel (right). A reliable and stable counting rate can only be expected in the case of aluminum. The black area is above the gate of the readout electronics.

near the lower edge of the second peak. To avoid the saturation of the readout electronics of the photomultipliers, limited to  $\sim 3$  MHz while  $\dot{n}_{loss} \sim 1$  GHz, the counters were placed 90 cm above the beam line and at  $\Delta s = 65$  cm downstream of the centre of the collimator where the rate exhibits a broad maximum with  $\Delta s$ . The counters are almost insensitive to a position error and the simulated yield is  $Y_{pm} \approx 3 \cdot 10^{-3}$  (Aluminum jaws), with a maximum rate in operation  $\dot{n}_{pm} = Y_{pm} \dot{n}_{loss} \approx 1.5 \cdot 10^6 \text{ counts s}^{-1}$ . The counters were calibrated in a high energy muon beam of the SPS where we fixed the trigger threshold of each counter by building a 'plateau curve'.

### 3.2 Data taking

The transverse position  $n_i$  of the jaws is given in normalised or r.m.s. beam units  $\sigma = (\varepsilon\beta)^{1/2}$  assuming a normalised emittance  $\varepsilon_o = 15 \mu\text{m}$ . We use the notation  $n_{1,2,3,v}$  for the primary, secondary, tertiary and vertical collimators. The nominal positions are  $n_1 = 6$ ,  $n_2 = 7$ ,  $n_3 = 9$  and  $n_v = 8$ . At the horizontal collimators  $\Delta n_i = 1$  is equivalent to  $\sigma_x = 1.6$  mm with  $\beta_h = 21.5$  m. We recorded the rates of the four counters, varying  $n_2$  (secondary retraction) by steps  $\delta n = 0.5$  in the range  $n \in [6, 12]$ . Then we varied  $n_3$  (tertiary retraction) in the range  $n \in [7, 13]$  with  $n_2 = 7$ .

Our data were recorded with the COLMON system [7]. It allows to accumulate counts of the photomultipliers during an adjustable time window repeatedly along the 14 seconds of the main cycle of the SPS. We fixed the time window to  $dt = 4 \cdot 10^{-2}$  s to be able to detect unwanted fast fluctuations of the losses during a measurement. The data were displayed on-line and stored for off-line analysis.

The origin of the  $n_i$  scales is found at every collimator by removing all the other jaws except one. Then, its opposite jaw is pushed towards the beam by small steps, until a spike of losses indicates that it is more inside the aperture than the fixed one. The closed orbit  $CO$  at the collimator is then the average of the two positions. We estimate the

error to  $\sigma(CO) \approx 0.2$  mm.

## 4 SIMULATION OF THE EXPERIMENT

The simulation of the experiment is made with our K2 code and GEANT. In the main loop of the code, we start tracking a proton of initial amplitude  $A < n_1$  and random betatronic phases with a one-turn linear matrix, to which an average increase of horizontal amplitude is applied at each turn which corresponds to the kicker noise (Section 3). When a collimator is touched, detailed tracking of elastic scattering is done (Section 4.1). Then the proton is tracked by linear matrices between collimators. Whenever an inelastic interaction occurs, the tracking is stopped and the coordinates of the proton stored for later simulation of their detection (Section 3.1). At the end of the cleaning section, an amplitude analysis allows to know if the proton will be lost at the aperture limitation of the ring. Then the tracking is stopped or a turn is closed and the tracking continues if the particle was not absorbed. We ran K2 and GEANT for every set of  $n_i$  positions. Many small effects on the data are taken into account including the variation of the GEANT yields  $Y_{pm}$  with the distance between two opposite jaws or with the impact parameter distribution changing with different relative retractions.

### 4.1 Elastic scattering processes

We only briefly review the scattering processes treated in K2. An extended discussion will appear later [11].

**Coulomb and multiple coulomb scattering** The differential cross-section of Coulomb scattering is  $d\sigma_c/dt = 2.61 \cdot 10^{-4} Z^2 G(t)/t^2$  with  $G(t) = \exp(-0.86R^2t)$  the electromagnetic form factor of the nucleus,  $t = (p\theta)^2$  the momentum transfer,  $\theta$  the polar angle of diffusion and  $R$  the nuclear radius. At small  $t$  the cross-section diverges, with a resulting finite effect which can be treated as a diffusion process, called multiple Coulomb, or Moliere scattering [9]. The r.m.s. of the projected angle  $\theta$  and of the transverse offset  $\Delta$  after the traversal of a length  $s$  through a material of radiation length  $L_R$  are given by (with units m and TeV/c)

$$\theta_o(s) = \frac{13.6 \cdot 10^{-6}}{p} \left(\frac{s}{L_R}\right)^{1/2}, \quad \Delta_o(s) = \frac{\theta_{mcs}^o s}{\sqrt{3}}. \quad (2)$$

Arbitrary large  $s$  steps can be made without biasing the results by using the correlation factor  $\rho_{\theta\Delta} = \sqrt{3}/2$ . Both distributions  $dN/d\theta$  and  $dN/d\Delta$  are Gaussian up to  $\approx 3\sigma$ . Beyond, Coulomb scattering proper takes over. The special treatment of multiple coulomb scattering near the edge of a jaw will be found in [11].

**Nuclear elastic scattering** Nuclear elastic processes are point-like interactions described by an optical model. The angular distribution of the scattered protons is Gaussian to a good precision. Its standard deviation is related to

the effective radius  $R_{eff}$  of the proton-target compound. The angular distribution is written

$$\frac{d\sigma}{dt} = \sigma_{el} b e^{-bt} \quad (3)$$

with  $\sigma_{el}$  the elastic cross-section and  $b = 0.16 R_{eff}^2 [(GeV/c^2)^2, \text{fermi}]$  the slope parameter. A proton can scatter both on nuclei and on nucleons inside the nucleus. Proton and neutrons are treated identically. In addition to elastic scattering, the incident proton do diffractive dissociation on nucleons, a process which is marginal at 120 GeV.

**Proton-nucleon elastic scattering** In the TeV range (LAB frame), where (3) applies well,  $\sigma_{pp,el} \approx 8.5 \text{ mb}$  and  $b \approx 13 \text{ GeV}^{-2}$ , neglecting a weak dependence of  $\sigma$  and  $b$  with momentum. Comparing pN and pp data, we deduce that  $pp$  elastic scattering is not visibly modified when occurring inside a nucleus. In particular, no trace of double elastic scattering is observed. The equivalent number of free scatterers in a nucleus can be given by  $n_{pn} = 1.56 A^{1/3}$  [11]. The  $pn$  elastic cross-section is then  $\sigma_{pn}(A) = n_{pn} \sigma_{pp,el}$ .

**Proton-nucleus scattering** Total and elastic proton-nucleus ( $pN$ ) cross-sections are reported in [9]. They are almost constant in the few hundred GeV/c momentum range. Differential elastic cross-section are found in [10]. Non measured data can be interpolated with  $A^{1/3}$  or  $A^{2/3}$  laws, which fit well the data [11]. Formula (3) is adequate to fit the data, except for very heavy nuclei where secondary and tertiary diffraction peaks of marginal importance are visible.

## 5 ANALYSIS AND RESULTS

A useful measurement of the ratio of interactions in a collimator and of the beam loss rate requires an accuracy  $\dot{I}/I \sim 10^{-2} \dot{n}_{loss}/N_p = 5 \cdot 10^{-6}$ , while a beam current transformer offers at best  $\dot{I}/I \sim 5 \cdot 10^{-5}$  for short integration times. We rather computed the ratios  $r_i = N_i/(N_1 + N_2 + N_3)$  of the rates  $N_i$  measured at the three horizontal collimators. The data are presented in Figure 3, together with the same values simulated with K2. The three identical assemblies of horizontal collimator and detector allow to compare directly the measured and the simulated data, without any free or simulated parameter. The use of loss rates at the vertical collimator is more delicate in that respect and was discarded from this preliminary analysis. During the MD session, we observed a beta-beating of 12% between  $HC1$  and  $HC2$ , by pushing inside a secondary jaw until it touches the primary halo defined by the primary collimator. Our effective  $n_2$  abscissa were corrected accordingly in the secondary-retraction experiment. This is the sole correction made to our data. No such effect was observed with the tertiary collimator. The relative error of the transverse scale for  $n_2$  and  $n_3$  relatively to  $n_1$  is estimated to  $\sigma(n)/n \approx 3\%$ . The error of the measured rates

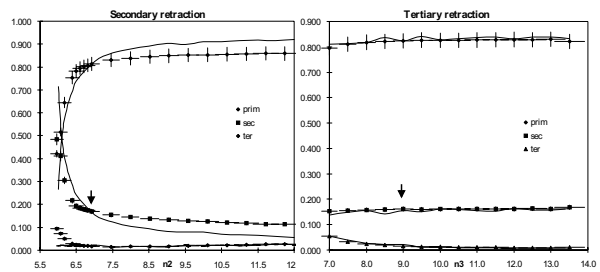


Figure 3: The measured rates  $r_i$  at the collimators. Left: the secondary jaw retraction data, right: the tertiary jaw retraction data. The vertical units are fractions of unity, see text. The dots are the measured values. The lines are obtained by the simulation described in the text. The small fluctuations are of statistical nature. The arrows indicate the position corresponding to the operation of the two-stage system with a ring aperture of  $\approx 9\sigma$ .

is estimated to  $\sigma(N_i)/N_i \approx 3.5\%$  and is the quadratic sum of the uncertainties related to the primary impact parameter range (2%), the possible drift of the gate of the PM's (2.5%) and the scintillator location and effective size (2%).

Last year [2] we reported the result of a former set of data, where the agreement between data and simulation was obtained with two floating constants. We found a defective calibration of one counter, and the use of a too small emittance to compute transverse locations resulted in too closed collimators, producing enough losses to avoid the use of noise, but inducing primary losses at the vertical collimator, thus biasing the data. Both effects were corrected for the present measurements.

The present results are very good, especially at the tertiary collimator, making us confident that our simulated efficiencies of the LHC collimation system [2] are reliable.

## 6 ACKNOWLEDGMENTS

We thank R. Jung for providing us with collimators which nicely fit our needs and C. Arimatea, A. Ferrari, J.J. Gras, W. Hofle and H. Jakob for their help during the data taking.

## 7 REFERENCES

- [1] The Large Hadron Collider, CERN/AC/95-05(LHC), 1995.
- [2] N.Catalan Lasheras et al., proc.symp. 'Near Beam Physics', Fermilab, Sept. 1997, and CERN LHC Proj.Rep. 156,1998.
- [3] T.Trenkler and J.B.Jeanneret, Part.Acc.,50,287(1995).
- [4] D.I. Kaltchev et al., PAC97, Vancouver, June 1997 and CERN LHC Proj.Rep.134,1997.
- [5] J.B.Jeanneret, these proceedings, abstract MOP06C.
- [6] W. Hofle, Private communication, November 1997.
- [7] J.J. Gras and G. Ferioli, CERN-SL-97-73(BI), 1997.
- [8] GEANT, Application Software Group, CERN, March 1995.
- [9] Review of Particle Properties, Phys.Rev. D45, 1992.
- [10] A.Schiz et al., Phys.Rev.D21, p.3010, 1980.
- [11] to appear in N.Catalan Lasheras, Ph.D. thesis, 1998.